J Mater Sci: Mater Med (2009) 20:1763–1770
DOI 10.1007/s10856-009-3733-1

# Mechanical examinations on dental implants with porous titanium coating

**H. Schiefer · M. Bram · H. P. Buchkremer · D. Stöver**

Received: 14 August 2007 / Accepted: 16 March 2009 / Published online: 26 March 2009


**Abstract** Due to its good biocompatibility, porous titanium is an interesting material for biomedical applications. Bone tissue can grow inside the porous structure and maintain a long and stable connection between the implant and the human bone. To investigate its long term stability, the mechanical behavior of porous titanium was tested under static and dynamic conditions and was compared to human bone tissue. A promising application of this material is the coating of dental implants. A manufacturing technique was developed and implants were produced. These implants were fatigue tested according to modified ISO 14801 and the micro structural change was examined. The fatigue test was statically modeled using finite element analysis (FEA). The results show that the implants resist a continuous load which is comparable to the loading conditions in the human jaw. The experiments show that the porous titanium has bone-like mechanical properties. Additionally the porous titanium shows an anisotropic behavior of its mechanical properties depending on the alignment of the pores. Finally, other potential applications of porous titanium are outlined.

## 1 Introduction

Today, most endosseous dental implants are screw-shaped. In the case of patients with ongoing bone resorption, longterm stable fixation of these implants becomes difficult. A promising solution to this problem is provided by dental implants with a porous coating. To ensure bone ingrowth, an interconnected pore system is necessary [1, 2]. The ideal pore size for the ingrowth of bone tissue and blood vessels lies in the range of 100–500 μm [3, 4]. The porosity should be at least 50% [5]. Bone-like mechanical properties of the implant material, particularly Young's Modulus are important factors in avoiding stress shielding [2]. Bone ingrowth in the porous coating means that a stable fixation of such dental implants is expected, even at a reduced implant length. Different techniques exist for the fabrication of dental implants with a porous coating: the sintering of larger spherical powder particles on a dense titanium core [6], microwave-sintering with a dense core and a gradient porosity [7], plasma-spraying on a titanium core [8], slip-casting with a titanium slurry on PU foam [9] and a slip-casting process with a polymer space holder (CSTi coating) [10]. Titanium and titanium alloys are preferred materials for implant applications because of their high specific strength and their good biocompatibility, which is due to the formation of a durable $TiO_2$ layer on its surface [11]. Titanium grade 4 and the $\alpha$-$\beta$-alloys Ti-6Al-4 V and Ti-6Al-7Nb are particularly well-known materials for dental implants [12]. The aim of this work is to adapt the space holder method for the manufacturing of dental implants with porous coatings and the evaluation of the mechanical properties of the porous titanium. The technique of fabricating porous titanium has been published elsewhere [13, 14]. After the manufacturing route for dental implants had been developed, these implants were examined by a modified fatigue test approaching ISO 14801. The stress distribution during the fatigue test was modeled using the FEA technique in order to identify the highest loaded regions of the dental implant components. The mechanical behavior was also tested for the FEA calculations of dental implants and for other potential

H. Schiefer (✉) · M. Bram · H. P. Buchkremer · D. Stöver
Institut für Energieforschung (IEF-1), Forschungszentrum Jülich GmbH, 52425 Jülich, Germany
e-mail: herwig_schiefer@web.de

applications of the porous titanium. Therefore Young's Modulus and the strength on the porous titanium in dependence of the pore size were measured under static conditions. The anisotropic mechanical behavior, which may have been caused by the manufacturing process, was also taken into consideration [15].

## 2 Experimental

### 2.1 Fabricating and testing porous titanium samples

For the fabrication of porous titanium samples, a mixture of 30 Vol.% titanium powder (grade 4, particle size <45 μm, supplier GfE, Nürnberg (Germany) produced by the HDH (hydrogenization–dehydrogenization) process and 70 Vol.% angular space holder (ammoniumhydrogencarbonate; $(NH_4)HCO_3$; particle size fraction 125–250 and 355–500 μm) was uniaxially pressed to samples with a diameter of D = 60 mm and a height of H = 12 mm with a pressure of P = 350 MPa. To remove the space holder, the green bodies were annealed for 10 h at 150°C in air. After this, the samples were sintered at T = 1300°C for t = 3 h in argon atmosphere. The amount of impurities (e.g., C, N, O) was measured with a LECO-System (N and O: LECO TC-436 AR, C: LECO CS-344). The samples for the static compression tests were fabricated by electro-discharge machining with a diameter of D = 6 mm and a height of H = 9 mm. One part of the samples was cut parallel to the press-direction, the other part was cut perpendicular to this direction. Compression tests were performed on a universal testing machine in air at room temperature. The relative strain was conductively measured with sensors at the pressure plates. Each sample was compressed to a strain of $\varepsilon = 50\%$, the crosshead speed was 0.5 mm/min. Young's Modulus and the $\sigma_{0.2}$-strength were graphically determined from the elastic regime of the stress-strain curve.

In order to examine the porous titanium mixtures with small (125–250 μm) and large (355–500 μm) spacer particles, they were cold isostatically pressed to cylinders in a rubber mould in a water-oil emulsion with a pressure of P = 350 MPa. After the spacer had been removed and sintering had been performed at 1300°C for 3 h, the samples for the fatigue test were cut into cylinders with a diameter of D = 10 mm and a height of H = 15 mm by electro-discharge machining. The fatigue testing was performed using a "Schenk Zug-Druckpulser PHG N" testing machine with a frequency of f = 50 Hz and $R = \sigma_{min}/\sigma_{max} = 0.1$. The samples were tested at pressures between 40 and 87.5% of the $\sigma_{0.2}$-strength of the porous titanium. The experiment was stopped after 4.3 $10^6$ cycles and the plastic deformation of the samples was measured with a calliper. Additionally with its mass the geometric porosity P [%] of the porous titanium samples was calculated according to $P = 1-(\rho_s/\rho_t)$ where $\rho_s$ is the density of the porous sample and $\rho_t$ the theoretical density of pure titanium (4.5 g/cm$^3$).

### 2.2 Fabricating dental implants with porous coating

Figure 1 shows two options for the fabrication of dental implants with porous coatings. In both cases, a mixture of titanium powder (30 Vol.%) and space holder (70 Vol.%) with a particle size fraction of 125–250 μm was cold isostatically pressed onto a titanium rod. The coating was near-net-shape machined by turning in the unsintered state. After the spacer was removed and sintering was performed, the samples were machined by drilling and sawing to achieve a tube with a porous coating. Finally, a dense titanium core with an internal screw thread was pressed into the tube part. In type 1 (Fig. 1a, c), the porous coating

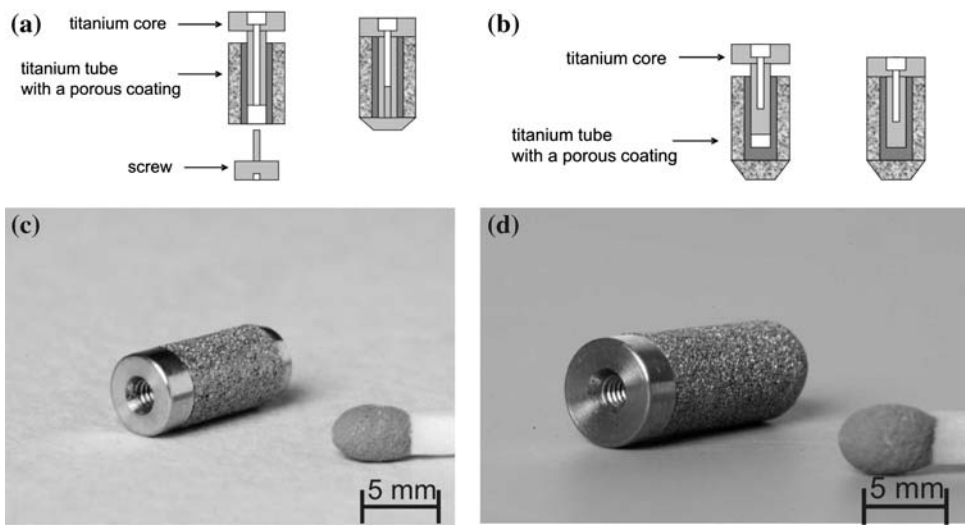


**Fig. 1** Dental implants with a porous coating, **a** schematic fabrication steps of type 1 using a screw for fixation, **b** schematic fabrication steps of type 2 fixation using adhesive joining. **c** type 1 with a massive tip, **d** type 2 with persistent porosity

was fixed by a screw on the tip of the implant. After joining, the screw was machined by turning to achieve a cone-like tip and roughened by sandblasting. Type 2 was adhesively joined and allows the joint between the titanium core and the porous tube to be improved by conjoining both components by electron-beam welding at the interface (Fig. 1b, d). Two types of dental implants were developed because to survey two different kinds of manufacturing methods. The diameter of each type was 5 mm, the height was 12 mm.

### 2.3 Fatigue testing of dental implants

The dental implants underwent a fatigue test approaching modified ISO 14801 (Fig. 2). Since the dental implant was at an early state of development, the test was modified by applying the force directly onto the massive titanium head of the implants. For this test, the porous dental implants were embedded in araldite under vacuum conditions to infiltrate the porous structure. To simulate an extreme loading condition, which may occur in cases of ongoing bone resorption, the porous coating hangs 3 mm over the edge of the polymer bush. The force was applied with a plunger directly to the head of the implant in an angle of 30°. The tests were performed at a temperature of T = 37°C in a physiological 0.9% NaCl solution. The implants were tested up to 2 $10^6$ cycles with a frequency of 2 Hz with different loading conditions of F = 200 und 300 N. After the test, the failure behavior of the implants was examinated with optical microscopy on an embedded grinding.

### 2.4 FEA modelling

Due to the similarity of the results of the FEA modelling for both implant types, only the results of implant type 2 are shown here. The implants were designed with the CAD-software "CATIA V5". For the calculations, the program "ANSYS 10.0 workbench" was used. Figure 3 exhibits the components of type 2 considered in the model: titanium core, titanium bush, polymer resin (araldite) and porous titanium infiltrated with araldite. Meshing was

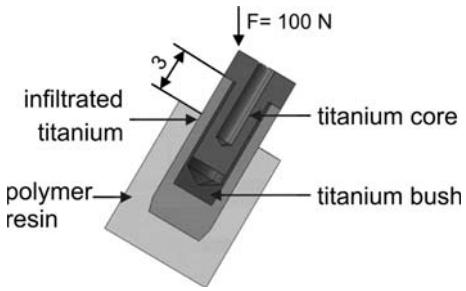


**Fig. 2** Geometry of dental implant type 2

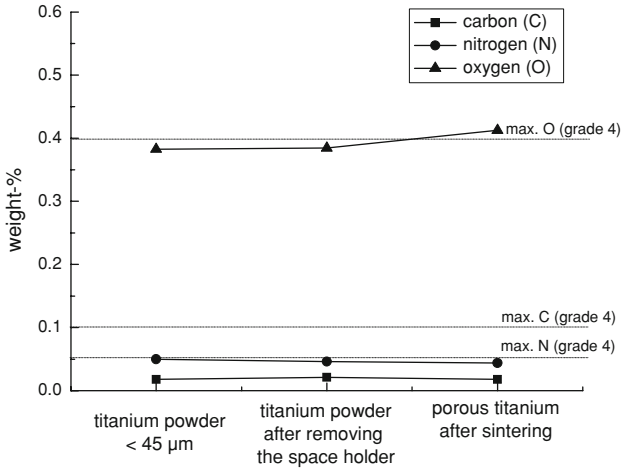


**Fig. 3** Chemical impurities of titanium after each fabrication step in the space holder method. The horizontal lines show the requirements for titanium grade 4 (max. content)

**Table 1** Parameters for FEA Modelling

| | E (GPa) | $\upsilon$ |
|---|---|---|
| Titanium | 105 | 0.31 |
| Infil. titanium | 6.4 | 0.33 |
| Polymer resin | 2.4 | 0.40 |

automatically done by the program. On the edge between implant-head and shaft the mesh was additionally refined. Calculations were performed for an implant load of F = 200 N at the edge of the massive titanium core at an angle of 30°. This force simulated a typical load for incisors [6]. Due to the fact that the calculations were performed with a half-model, the force was reduced to F = 100 N. Table 1 summarizes the parameters (E = Young's Modulus, $\upsilon$ = Poissons ratio), which were used for the linear-elastic calculation. The examinations of these materials were done on test samples with the same parameters under pressure load. The contact conditions are as follows. A bonded contact was assumed between infiltrated titanium and polymer resin. Between the core-bush and core-infiltrated titanium, a friction contact with a friction coefficient of $\mu = 0.8$ was used. This relatively high friction coefficient shall consider the press fit between both components.

## 3 Results

### 3.1 Chemical analysis of titanium

Figure 3 shows the carbon, oxygen and nitrogen contents of the titanium powder, the powder after the space holder was removed and the porous titanium after sintering. In

addition, the requirements for titanium grade 4 are also shown. Due to its fabrication process, the powder already has a high content of these impurities. After the annealing process for removing the space holder, a negligible increase in the amount of these elements occurs. No further distinct increase in the oxygen content was found until the sintering process, while the contents of nitrogen and carbon remained almost unchanged. As a consequence, the oxygen content of the porous titanium lay marginally over the requirements for titanium grade 4. A high content of these elements in the titanium does not impact on the biocompatibility of the titanium but it does embrittle the titanium matrix [16] thereby enhancing the risk of particle loss under dynamic load conditions.

### 3.2 Mechanical behavior of porous titanium

Figure 4a shows the stress-strain curve for porous titanium with a pore size of 125–250 µm and a porosity between 54.3% and 59.6%. The mechanical behavior of human bone tissue is also shown. The corticalis, the dense outer layer of the bone structure, shows a brittle fracture behavior. Contrary to this, the compacta, the inner, sponge-like bone tissue, is characterized by high elongation. The stress-strain curve of the porous titanium samples lies between the curves for the corticalis and compacta and can be adjusted well by varying the porosity.

Figure 4b shows the same information for porous titanium with a pore size of 355–500 µm. The higher porosity of all samples is surprising, since the same amount of space holder particles and the same sintering parameters were used as for small space holder particles. One possible explanation could be that the larger space holder particles cause the compaction behavior of the green body to deteriorate resulting in a higher porosity of the samples after sintering. Comparing the influence of fine and coarse space holder particles on the mechanical properties, the anisotropy of microstructure and therefore also the anisotropy of the deformation behaviour is clearly higher in case of coarse particles. Smaller space holder particles are preferred, if the main requirement of the application is a homogeneous deformation behaviour in all spatial directions. Figure 5 shows a SEM picture of the pore structure of porous titanium with a pore size of 355–500 µm. If this picture shows mainly separated pores, the author in [15] shows that porous titanium with a comparable amount of space holder leads to an open porous foam. Additionally authors in [17] show that bone tissue can growth inside a porous titanium body with comparable properties. The white arrows indicate the compaction direction. It is obvious that there is a preferred orientation of the pores in a horizontal direction, which results from an alignment of the space holder particles during compaction.

The porous titanium samples show a typical elastic-plastic deformation behavior like the metallic foams in [18, 19]. The curve can be devided in 3 sections: linear-elastic, plateau and densification. Because of its relatively wide pore distribution the sections have a fluent transition between each other.

### 3.3 Fatigue testing of porous titanium

Figure 6 summarizes the results of the fatigue testing of porous titanium with different pore sizes. Below a pressure

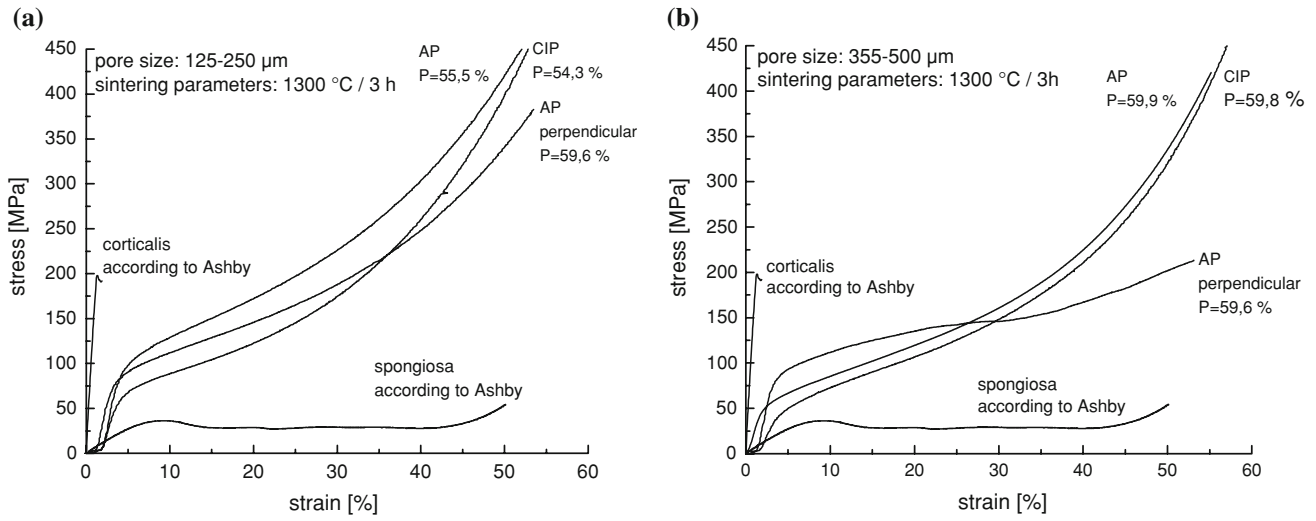


**Fig. 4** **a** Stress-strain behavior of porous titanium with a pore size of 125–250 µm compared to the mechanical behavior of human bone tissue according to Ashby [18]. AP means uniaxially pressed titanium, CIP means cold-isostatically pressed titanium. **b** Stress-strain behavior of porous titanium with a pore size of 355–500 µm compared to the mechanical behavior of human bone tissue according to Ashby [18]. AP means uniaxially pressed titanium, CIP means cold-isostatically pressed titanium

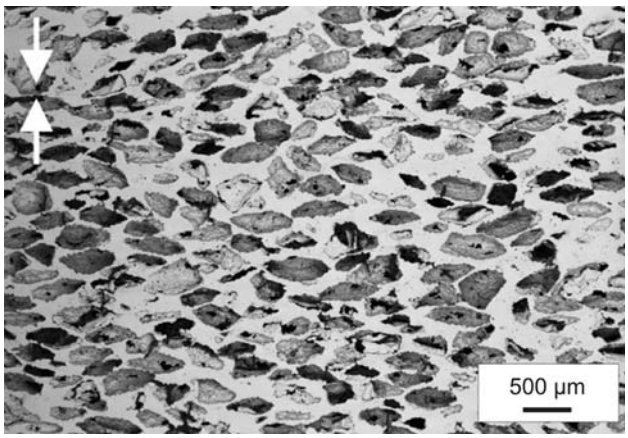


**Fig. 5** Uniaxially pressed porous titanium with preferred alignment of the pores perpendicular to the compaction direction (*white arrows*) of the greenbody. Pore size of the space holder fraction was 355–500 µm

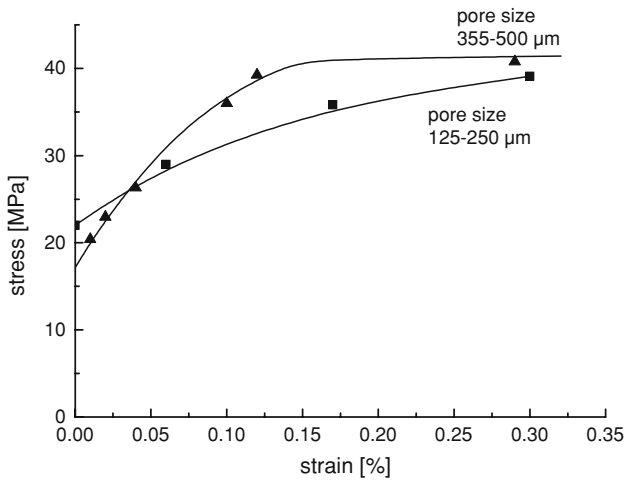


**Fig. 6** Irreversible deformation of porous titanium with different pore sizes after a fatigue test with at least 4 $10^6$ cycles at different stresses

of about 20 MPa (50% of the $\sigma_{0.2}$-strength of the porous titanium), no plastic deformation of the samples was found. An increase in the load is coupled with the occurence of irreversible plastic deformation. During fatigue testing, irreversible deformation was already found at stresses below $\sigma_{0.2}$, which increases disproportionately if the stress approaches $\sigma_{0.2}$. Even if this behaviour is not completely understood, it is assumed that there is an influence of the inhomogeneous distribution of wall thicknesses of sintered struts (compare Fig. 2). Areas, where the amount of thin struts prevails may deform already plastically at stresses below $\sigma_{0.2}$, while the predominant rest of the sample is still in the elastic regime. If the stress approaches the $\sigma_{0.2}$ value, an uniform plastic deformation of the samples becomes dominant coupled with the disproportionate increase of the deformation value. It should be noted that the average

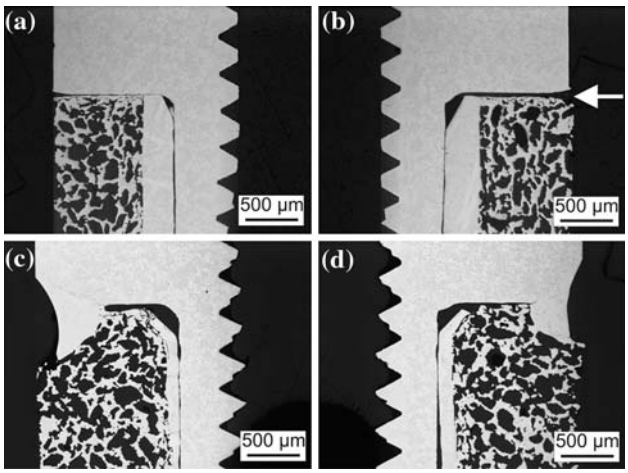


**Fig. 7** **a**, **b** Implant type 1 after the fatigue test with F = 300 N and 2 $10^6$ cycles. Formation of a notch (*arrow*) opposite the point where the load is applied. **c**, **d** Implant type 2 with an additional weld seam between the massive titanium head and the porous structure after the fatigue test with F = 300 N and 2 $10^6$ cycles

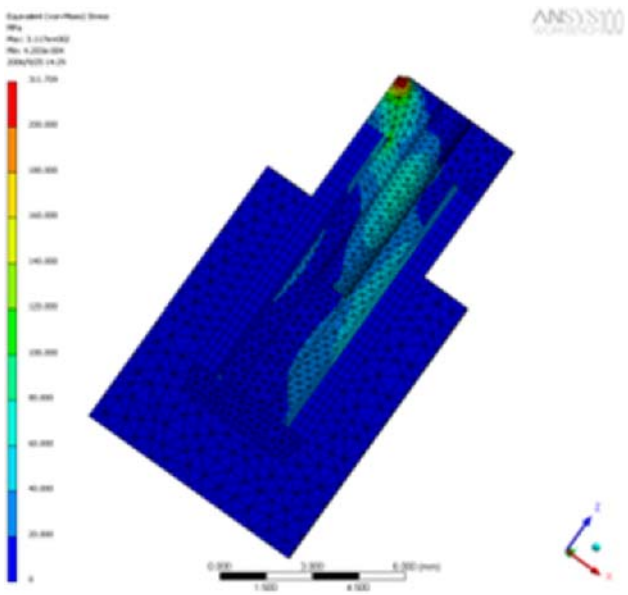

**Fig. 8** Von Mises stresses in dental implant type 2 with a loading of F = 200 N

weight loss of the samples with coarse pores at each loading level was 0.07%, even at low stresses, while the samples with smaller pores did not show any weight loss. Examinations of the lost particles with EDX revealed a high amount of copper and zinc, indicating that they are residuals from the electro-discharge machining of the samples. Therefore, electro-discharge machining would appear to be unsuitable for the shaping of porous titanium implants.

The fatigue tests were done according the suggestions in [19]. Actually there are only a few results of the fatigue

behavior of metallic foams. These results depending strongly on parameters like e.g., loading conditions, sample geometry, materials and fabrication techniques. Thus a comparison with of the results which were shown here is actually not possible.

### 3.4 Fatigue testing of dental implants

After at least 2 $10^6$ cycles and a maximum force of F = 200 N, no macroscopic damage of the dental implants occured. The same result was found for samples loaded with F = 300 N. After the test, the samples were examined by light microscope. Figures 7a, b show the cross section of implant type 1. Due to the fact that turning was chosen as the fabricating process, the pores at the top side of the coating were closed. Coarse grains exist at the interface between the porous coating and the titanium bush indicates a good adherence of the porous coating. No clear damage to the structure was visible, but opposite the point where the load was applied, a notch between the head of the massive titanium core and the porous coating was found. This notch was probably caused by a slight distortion of the core during load cycling. The result was confirmed on implant type 2. Fatigue testing with F = 300 N resulted in no damage to the porous coating but it did result in a slight distortion of the core. To overcome this problem, an additional weld seam at the interface between the massive titanium head and the porous structure would be advantageous. This distortion of the titanium core in the bush was avoided (Fig. 7c, d).

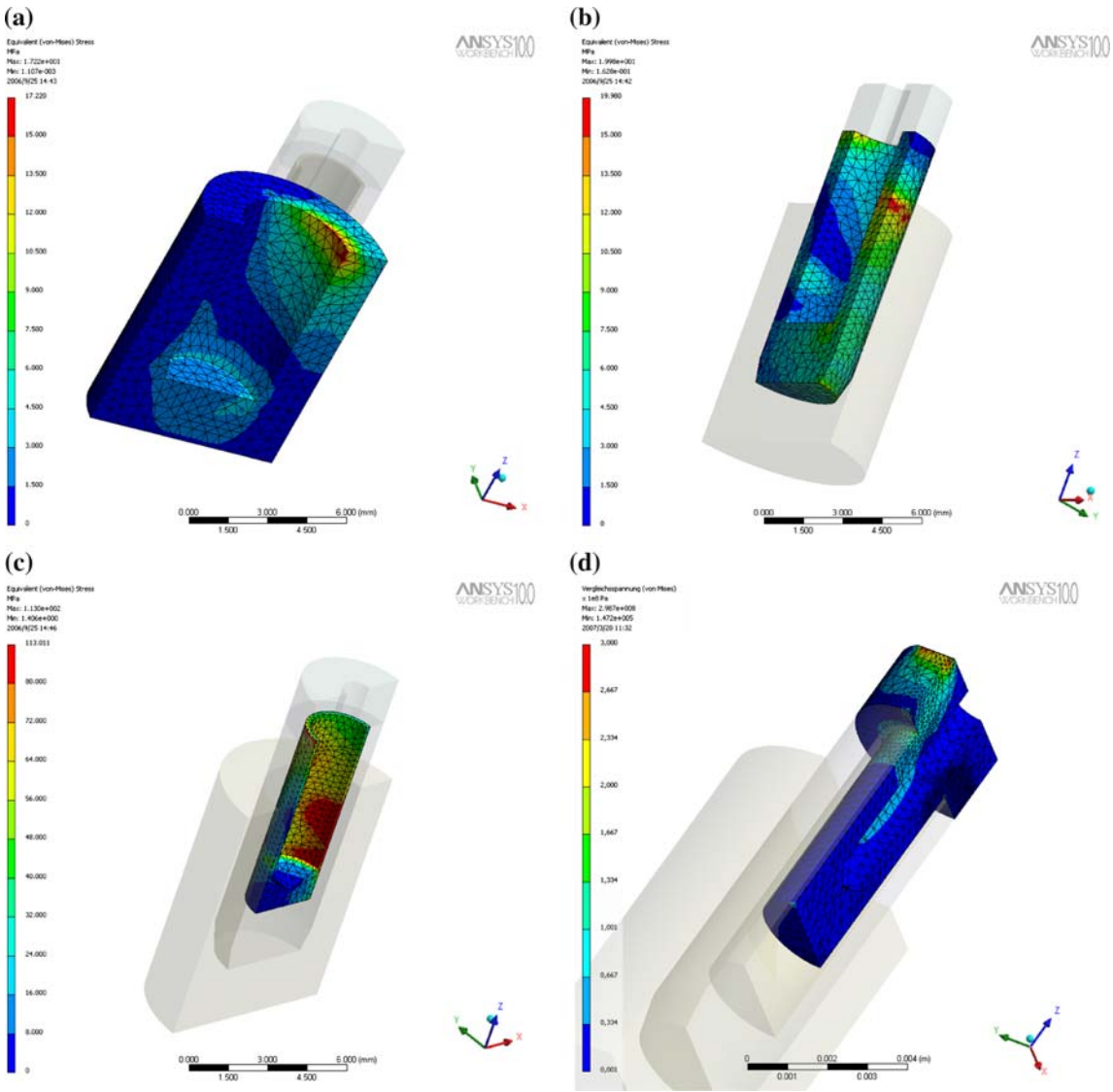


**Fig. 9** **a**, **b** Von Mises stresses of the components of implant type 2, **a** polymer resin, **b** infiltrated titanium, **c** titanium bush, **d** titanium core

**Table 2** Von Mises stresses of implant components of dental implants

| | Type 1 (MPa) | Type 2 (MPa) |
|---|---|---|
| Polymer resin | 27 | 15 |
| Titanium core | 130 | 154 |
| Titanium bush | 151 | 120 |
| Infiltrated titanium | 20 | 20 |

### 3.5 FEA modelling of the fatigue testing of dental implants

Figure 8 shows the Von Mises stresses for implant type 2, loaded with F = 200 N. The maximum stress occurs at the point where the load is exerted on the implant. The core and bush have to withstand the highest stresses, while the infiltrated titanium and polymer resin are almost unloaded. Figure 9 show the stress distribution of the implant components polymer-resin (Fig. 9a) and infiltrated titanium (Fig. 9b). The stress concentrations are generally opposite where the load is applied. Those regions where sharp-edged components are in contact with each other are relatively highly loaded. The bush experiences maximum loading at the edge, where the head of the massive titanium core comes into contact with it (Fig. 9c). Figure 9d shows the load distribution of the massive titanium core. As previously mentioned, the maximum stress occurs in the area where the load is exerted. Since this stress is of the same dimension for both implant types, the stress at the intersection between the head and the core was used for comparative purposes. Table 2 shows the Von Mises stresses of the components of both implants. Remarkably, the loading of the infiltrated titanium was the same. For implant type 1, the loading of the polymer resin and the titanium bush was higher than that of implant type 2. As a consequence, the loading of the titanium core is lower than that of implant type 2.

## 4 Conclusion

The mechanical properties of porous titanium, particularly the Young's Modulus lie between those of the human bone tissues compacta and spongiosa. The anisotropic behavior of the porous titanium was shown in a static compression test. This anisotropic behavior must be considered in the construction of implant devices. The fatigue strength of porous titanium was tested. When the load was lower than 50% of the $\sigma_{0.2}$-strength of the porous titanium (20 MPa), no plastic deformation occurred for more than 4 $10^6$ cycles. When the load was increased to 87% of the $\sigma_{0.2}$-strength, irreversible deformation of 0.3% occurred. Two types of dental implants with a porous coating, fabricated by the space holder method, were subjected to a modified fatigue test approaching ISO 14801. After 2 million cycles, no macroscopic damage was found in many of the tested implants. FEA calculations show equal loading conditions for both implant types. The massive titanium core and bush show the highest stresses of all implant components. Nevertheless, all components are loaded significantly below their $\sigma_{0.2}$-strength, therefore damage by overstraining is not expected under the conditions specified in ISO 14801.

The space holder technology has already been used for further biomedical applications such as implants for the spinal column. With the technology developed in this work, the range of applications may be widened to the porous coating of hip or knee implants to improve the connection with the surrounding bone.

**Acknowledgment** The authors would like to thank Dr. F. Schlottig and Dr. D. Snetivy of the Thommen Medical AG, Waldenburg (Switzerland) for helpful discussions and for conducting the fatigue tests on the dental implants. We would like to thank Professor P. Beiss, RWTH Aachen University, for conducting the fatigue tests on the porous titanium. We would like to thank U. Bänninger, ZH Winterthur, for his support with the FEM-analysis.

## References

1. Wen CE, Yamada Y, Shimojima K, Chino Y, Asahina T, Mabuchi M. Processing and mechanical properties of autogenous titanium implant materials. J. Mater Sci Mater Med. 2002; 13:397–401. doi:10.1023/A:1014344819558.
2. Thelen S, Barthelat F, Brinson LC. Mechanics considerations for microporous titanium as an orthopedic implant material. J. Biomed Mater Res A. 2004;69A:601–10. doi:10.1002/jbm.a.20100.
3. Triplett RG, Frohberg U, Sykaras N, Woody RD. Implant materials, design, and surface topographies: their influence on osseointegration of dental implants. J Long Term Eff Med Implants. 2003;13:485–501. doi:10.1615/JLongTermEffMedImplants.v13.i6.50.
4. Briggs EP, Walpole AR, Wilshaw PR, Karlsson M, Palsgard E. Formation of highly adherent nano-porous alumina on Ti-based substrates: a novel bone implant coating. J Mater Sci Mater Med. 2004;15:1021–9. doi:10.1023/B:JMSM.0000042688.33507.12.
5. Thieme M, Wieters K-P, Bergner F, Scharnweber D, Worch H, Ndop J, et al. Titanium powder sintering for preparation of a porous functionally graded material destined for orthopaedic implants. J Mater Sci Mater Med. 2001;12:225–31. doi:10.1023/A:1008958914818.
6. Asaoka K, Kuwayama N, Okuno O, Miura I. Mechanical properties and biomechanical compatibility of porous titanium for dental implants. J Biomed Mater Res. 1985;19:699–713. doi:10.1002/jbm.820190609.
7. Kutty MG, Bhaduri S, Bhaduri SB. Gradient surface porosity in titanium dental implants: relation between processing parameters and microstructure. J Mater Sci Mater Med. 2004;15:145–50. doi:10.1023/B:JMSM.0000011815.50383.bd.
8. Yang YZ, Tian JM, Tian JT, Chen ZQ, Deng XJ, Zhang DH. Preparation of graded porous titanium coatings on titanium implant materials by plasma spraying. J Biomed Mater Res. 2000;52:333–7. doi:10.1002/1097-4636(200011)52:2<333::AID-JBM12>3.0.CO;2-T.

9. Li JP, De Groot K. Proceedings in 10th World Conference on Titanium, Hamburg, 13–18 July 2003, p. 1–7.
10. Story BJ, Wagner WR. Zahnimplantate: schraube oder zylinder? Sulzer Tech Rev. 1998;1:38–40.
11. Eisenbarth E, Velten D, Schenk-Meuser K, Linez P, Biehl V, Duschner H, et al. Interactions between cells and titanium surfaces. Biomol Eng. 2002;19:243–9. doi:10.1016/S1389-0344(02)00032-1.
12. Niinomi M. Recent research and development in titanium alloys for biomedical applications and healthcare goods. Sci Technol Adv Mater. 2003;4:445–54. doi:10.1016/j.stam.2003.09.002.
13. Laptev A, Bram M, Buchkremer HP, Stöver D. Study of production route for titanium parts combining very high porosity and complex shape. Powder Metallurgy. 2004;47:85–92. doi:10.1179/003258904225015536.
14. Laptev A, Vyal O, Bram M, Buchkremer HP, Stöver D. Green strength of powder compact provided for the production of highly porous titanium parts. Powder Metallurgy. 2005;48:358–64. doi:10.1179/174329005X73838.
15. Imwinkelried T. Mechanical properties of open-pore titanium foam. J Biomed Mater Res. 2007;81A:964–70. doi:10.1002/jbm.a.31118.
16. Ward-Close CM, Godfrey AB, Thompson SR. Advances in titanium alloy powder. Met Pow Rep. 2005;July/August:20–25.
17. Steffen T, Krygier JJ, Karabasz D, Bobyn JD. 51th Annual meeting of the orthopaedic research society, Poster no. 1396 (2005).
18. Gibson LJ, Ashby MF. Cellular solids–Structure and properties. Cambridge : Cambridge University Press; 1997.
19. Ashby MF, Evans A, Fleck NA, Gibson LJ, Hutchinson JW. Wadley HNG metal foams–a design guide. UK: Butterworth Heinemann; 2000.